Spatial averaging for light reflection and transmission through cold-atom arrays

F. Robicheaux *

Department of Physics and Astronomy, Purdue University, West Lafayette, Indiana 47907, USA;
Purdue Quantum Science and Engineering Institute, Purdue University, West Lafayette, Indiana 47907, USA;
and ITAMP, Center for Astrophysics | Harvard & Smithsonian, Cambridge, Massachusetts 02138, USA

(Received 24 October 2024; accepted 6 January 2025; published 17 January 2025)

We theoretically and computationally investigate the role that the spatial spread of atoms plays in the transmission and reflection of weak light from atom arrays. In particular, we investigate whether coherent wave functions for the atoms' positions leads to different results from a thermal distribution with the same spatial spread. We find that the coherence is not relevant when the light is weak and the electronic states evolve on timescales shorter than the oscillation period of the atoms in their traps. Full numerical calculations and derivations using the sudden approximation show that reflection and transmission agree with the simple averaging over atom positions for these conditions. For parameters outside these restrictions, the simple spatial averaging may lead to inaccurate results.

DOI: 10.1103/PhysRevA.111.013711

I. INTRODUCTION

Inspired by theoretical and experimental advances, several groups have investigated scenarios involving light interacting with many atoms in regular arrangements [1–69]. Exciting possibilities arise when the separation of atoms is less than a wavelength of the light. Most of the theoretical investigations assumed the atoms were on a perfect grid with zero spatial deviation [1–55]. While this was useful for exploring basic concepts, it was not possible in practice: the wave function for the center-of-mass motion must at least have a spread from the ground-state wave function. For atoms not cooled to the motional ground state, the spread in positions was larger and many treatments averaged over spatial distributions in addition to treating the perfect lattice [56–69]. There was a wide range of applications for arrays of atoms including clocks [1–3], mirrors, light manipulation, and excitations on a lattice [4–43,58–67], collective Lamb shift [56], and quantum information applications [44–55,57]. Recent overviews covered important aspects of atom arrays [68,69].

Some of the calculations treated spatial deviations by fixing the atoms in space with random positions given by the spatial distribution function and averaging over the possible positions. While this prescription was reasonable, there has not been a clear derivation of how the spread of positions should be treated, especially in the limit the atoms were cooled to the motional ground state. Does the coherence of the vibrational wave function require special treatment? At a technical level, are the results the same for two cases where the spatial part of the density matrix has diagonal $\rho(x,x)$ the same but off-diagonal $\rho(x,x')$ substantially different? The purpose of this paper is to provide a clear derivation and numerical examples of how to treat the spatial spread of atoms in arrays. The examples we give will be for when the light and atoms reach steady state although this condition is not necessary.

For a general treatment, one of the conditions needs to be that the atoms scatter or reflect few photons while they evolve into the electronic steady state. If this condition is not satisfied, the wave function or density matrix associated with the atoms' positions will evolve. This clearly leads to results that do not solely depend on the positions of the atoms fixed in space. Typically, the scattering or reflection leads to heating the spatial degrees of freedom although special detuning and geometry could lead to cooling. This condition can be satisfied by decreasing the intensity of the incident light. Therefore, except for very subradiant cases, the approximation will work well when the one atom Rabi frequency is much less than the one atom decay rate: $\Omega \ll \Gamma$.

The treatment below will focus on the case where the trap frequency ω_t is much less than the decay rate of the system. Except for very subradiant cases, this leads to $\omega_t \ll \Gamma$. In typical atom traps, the trap frequency in the plane of the atom array is different from that perpendicular to the plane of the atom array. Often, the in-plane frequency is larger than that perpendicular to the plane, leading to a direction dependence to ω_t. For the condition $\omega_t \ll \Gamma$, the largest of the frequencies should be used. Most experimental arrangements will satisfy this condition. We also make this restriction because smaller ω_t leads to larger spatial spreads which are more crucial to treat correctly.

We show that within these conditions an accurate, approximate treatment of the light plus atom system is to calculate the light properties for atoms fixed in space and then average the light properties over the positions of the atoms weighted by their position distribution. We use the sudden approximation to derive this result, Sec. III, hence the condition that the atoms do not move substantially for the duration of the light-atom interaction. We also numerically compute the reflection and transmission in simple cases using a full density matrix

*Contact author: robichf@purdue.edu

treatment, Sec. IV, to illustrate the accuracy of the fixed in space approximation. The numerical treatment is the same whether the spread in positions is from being in a thermal state or being in one vibrational eigenstate. Restricting the density matrix calculation to the ground vibrational state is a different approximation that can lead to qualitatively wrong changes in the properties of the light (transmission, reflection, etc.). For example, we describe a case in Sec. IV where even if the recoil energy is 3000 times smaller than the vibrational energy spacing, performing a density matrix calculation with all atoms restricted to the vibrational ground state leads to qualitatively wrong changes in the light properties.

II. METHOD

In this section, we describe the method used for the numerical calculation. In addition, there are descriptions of the interaction of many atoms with light in a three-dimensional vacuum and in a one-dimensional waveguide.

A. Full density matrix

To account for the motion of the atoms as well as the evolution of their internal states, we will use a density matrix formalism which expands the density matrix in a basis of vibrational states for the atoms' motion and internal states. We will use the formalism described in Ref. [70] with one exception described in the Appendix. Also, we will slightly change some of the notation to avoid confusion of the role of indices.

The calculations will be for N atoms that are trapped in harmonic wells. To simplify the role of the electronic states, we will only consider two electronic states for each atom, j: $|g_j\rangle$ and $|e_j\rangle$. These lead to the definition of electronic operators for atom j,

$$\hat{e}_j \equiv |e_j\rangle\langle e_j|, \quad \hat{\sigma}_j^- \equiv |g_j\rangle\langle e_j|, \quad \hat{\sigma}_j^+ \equiv |e_j\rangle\langle g_j|. \tag{1}$$

The position for the center of the atom trap for atom j will be denoted $\boldsymbol{R}_j$ and the operator for the atom position relative to the trap center will be denoted $\boldsymbol{r}_j$. We will assume that the trap frequency could be different for different directions, but we will denote the angular frequency generically by ω_t. The harmonic oscillator eigenstate for atom j will be denoted $|n_j\rangle$; where necessary, the eigenstate for each of the x, y, z directions will be noted. The light has a wave number k_0; when the atoms interact with a plane light wave the wave vector will be $\boldsymbol{k}_0$. Because the atoms interact through the electromagnetic field an important position operator is $k_0\boldsymbol{r}_j$ which, for each direction, has the form $\eta(\hat{a}_j + \hat{a}_j^\dagger)$ with $\hat{a}_j$ the vibrational lowering operator for the jth atom. The constant $\eta = k_0\sqrt{\hbar/(2M\omega_t)}$ with M the atom's mass; we are interested in the Lamb-Dicke regime $\eta \ll 1$ so the spread in positions can be less than the wavelength.

We numerically solve the density matrix equation

$$\frac{d\hat{\rho}}{dt} = \frac{1}{i\hbar}[\hat{H}, \hat{\rho}] + \mathcal{L}(\hat{\rho}), \tag{2}$$

with $\hat{\rho}$ the density matrix of the system, $\hat{H}$ is the Hamiltonian, and $\mathcal{L}(\hat{\rho})$ is the Lindblad superoperator. The Hamiltonian consists of three terms

$$\hat{H} = \hat{H}_0 + \hat{H}_L + \hat{H}_{dd}, \tag{3}$$

where the $\hat{H}_0$ is for the atom traps plus the energy of the electronic states, the $\hat{H}_L$ is for the laser-atom interaction in the rotating wave approximation for an incident plane wave with wave vector $\boldsymbol{k}_0$, and $\hat{H}_{dd}$ is for the dipole-dipole interaction. These terms have the following form:

$$\hat{H}_0 = \hbar\sum_j[\omega_t(\hat{a}_j^\dagger\hat{a}_j + 1/2) - \Delta\hat{e}_j], \tag{4}$$

$$\hat{H}_L = \hbar\sum_j \frac{\Omega}{2}\left(e^{i\boldsymbol{k}_0(\boldsymbol{R}_j+\boldsymbol{r}_j)}\hat{\sigma}_j^+ + e^{-i\boldsymbol{k}_0(\boldsymbol{R}_j+\boldsymbol{r}_j)}\hat{\sigma}_j^-\right), \tag{5}$$

$$\hat{H}_{dd} = \hbar\sum_{j\neq j'}\hat{\Omega}_{jj'}\hat{\sigma}_j^+\hat{\sigma}_{j'}^-, \tag{6}$$

where ω_t is the trap frequency, Δ is the detuning of the laser from the transition $\Delta = k_0c - (E_e - E_g)/\hbar$, Ω is the Rabi frequency, and $\hat{\Omega}_{jj'}$ is the position operator-dependent part of the dipole-dipole interaction, Eq. (8). If the incident light is different from a plane wave (for example, a focused beam), then the spatial terms in Eq. (5) are modified. The Lindblad superoperator term is

$$\mathcal{L}(\hat{\rho}) = \sum_{jj'}\left(\hat{\sigma}_j^-\hat{\Gamma}_{jj'}(\hat{\rho})\hat{\sigma}_{j'}^+ - \frac{1}{2}\{\hat{\sigma}_{j'}^+\hat{\sigma}_j^-\hat{\Gamma}_{jj'}, \hat{\rho}\}\right), \tag{7}$$

where $\{\hat{O}_1, \hat{O}_2\} = \hat{O}_1\hat{O}_2 + \hat{O}_2\hat{O}_1$ for any two operators and $\hat{\Gamma}_{jj'}$ is the position operator-dependent part of the dipole-dipole interaction, Eq. (9).

For atoms interacting in three dimensions far from any surfaces, the Hamiltonian part of the dipole-dipole operator is

$$\hat{\Omega}_{jj'} = \frac{\Gamma}{2}\left[n_0(s_{jj'}) + \frac{3(\hat{\boldsymbol{s}}_{jj'}\boldsymbol{q})(\hat{\boldsymbol{s}}_{jj'}\boldsymbol{q}^*) - 1}{2}n_2(\hat{s}_{jj'})\right], \tag{8}$$

where the $n_\ell(x)$ are the Neumann functions, $\boldsymbol{q}$ is the unit vector for the dipole orientation, $s_{jj'} = k_0|\boldsymbol{R}_j + \boldsymbol{r}_j - \boldsymbol{R}_{j'} - \boldsymbol{r}_{j'}|$ and $\hat{s}_{jj'}$ is the unit vector for the atom difference. Because of the presence of the $\boldsymbol{r}_j$ and $\boldsymbol{r}_{j'}$, the $\hat{\Omega}_{jj'}$ is an operator that can change the vibrational quantum numbers of atoms j and j'. The Lindbladian part of the dipole-dipole operator is

$$\hat{\Gamma}_{jj'} = \Gamma\left[j_0(s_{jj'}) + \frac{3(\hat{\boldsymbol{s}}_{jj'}\boldsymbol{q})(\hat{\boldsymbol{s}}_{jj'}\boldsymbol{q}^*) - 1}{2}j_2(\hat{s}_{jj'})\right], \tag{9}$$

with the $j_\ell(x)$ the spherical Bessel functions. Using $h_0^{(1)}(s) = e^{is}/[is]$ and $h_2^{(1)}(s) = (-3i/s^3 - 3/s^2 + i/s)e^{is}j_\ell(s) = \mathrm{Re}[h_\ell^{(1)}(s)]$ and $n_\ell(s) = \mathrm{Im}[h_\ell^{(1)}(s)]$. Similar to the $\hat{\Omega}_{jj'}$, the $\hat{\Gamma}_{jj'}$ is an operator due to the presence of the $\boldsymbol{r}_j$ and $\boldsymbol{r}_{j'}$ and can change vibrational quantum numbers. The trickiest part is the first term of Eq. (7) where the $\boldsymbol{r}_j$ acts from the left on the density matrix while the $\boldsymbol{r}_{j'}$ acts from the right on the density matrix. See the more detailed discussion in Refs. [70–72].

For atoms that can only emit light into or absorb from a one dimensional wave guide, we will take the Hamiltonian part of the dipole-dipole operator as

$$\hat{\Omega}_{jj'} = \frac{\Gamma}{2}\sin(k_0|X_j + x_j - X_{j'} - x_{j'}|), \tag{10}$$

and

$$\hat{\Gamma}_{jj'} = \Gamma \cos(k_0[X_j + x_j - X_{j'} - x_{j'}]). \tag{11}$$

While these equations are simpler than those for light in three dimensions, they lead to the same basic physical processes: transmission and reflection of light, vibrational excitation or deexcitation, and so on.

We solve for the time-dependent density matrix using the eigenstates of the $\hat{H}_0$ operator, Eq. (4). We will define the state $|\alpha\rangle$ to be the tensor product of individual atom eigenstates. For atom j, we use i_j to be 0 or 1 for $|g_j\rangle$ or $|e_j\rangle$ and $|n_j\rangle$ the vibrational state of atom j which will be limited to the range 0 to $n_{\max} = N_{\rm vib} - 1$. This gives

$$|\alpha\rangle \equiv |i_1\rangle \otimes |n_1\rangle \otimes |i_2\rangle \otimes |n_2\rangle \otimes \cdots, \tag{12}$$

where there are $(2N_{\rm vib})^N$ states altogether. We define the density matrix as

$$\hat{\rho} = \sum_{\alpha\alpha'} |\alpha\rangle \rho_{\alpha\alpha'} \langle\alpha'|. \tag{13}$$

To evaluate an operator $\hat{O}$ acting on ρ, we use the representation

$$\langle\alpha|\hat{O}\hat{\rho}|\alpha'\rangle = \sum_{\alpha''} \langle\alpha|\hat{O}|\alpha''\rangle\langle\alpha''|\hat{\rho}|\alpha'\rangle, \tag{14}$$

which is relatively efficient because the operators in Eq. (2) are extremely sparse.

B. Transmitted and reflected light

Since we are interested in the effect of atoms' positions on the interaction of light, we also need to have a form for the operators that can be evaluated to compute the intensity of light at a position away from the atoms. The transmitted and reflected light in the steady state is somewhat undefined because, for most cases, the interaction with the light will lead to the atoms' motion heating with time. Strictly speaking, there is no steady state. However, in most experiments, it is assumed that the light is weak enough that the internal states of the atom reach steady state before vibrations appreciable change. Thus, we will investigate the reflection and transmission on this timescale by choosing the Rabi frequency to be much smaller than Γ in most of our examples.

For light in three dimensions, the calculation of the electromagnetic flux in the direction $\boldsymbol{\mu}$ at position $\boldsymbol{R}$ involves an electric-field-type operator with a form

$$\hat{\boldsymbol{E}}(\boldsymbol{R}) = \boldsymbol{E}_{cl}(\boldsymbol{R}) + \sum_j \hat{\sigma}_j^- \boldsymbol{g}_E(\boldsymbol{R} - \boldsymbol{R_j} - \boldsymbol{r_j}), \tag{15}$$

where $\boldsymbol{g}_E(\boldsymbol{R}) \propto [\boldsymbol{q} - \hat{\boldsymbol{R}}(\hat{\boldsymbol{R}} \cdot \boldsymbol{q})]h^{(1)}(kR)$ in the far-field- and a magnetic-field-type operator with a form

$$\hat{\boldsymbol{B}}(\boldsymbol{R}) = \boldsymbol{B}_{cl}(\boldsymbol{R}) + \sum_j \hat{\sigma}_j^- \boldsymbol{g}_B(\boldsymbol{R} - \boldsymbol{R_j} - \boldsymbol{r_j}), \tag{16}$$

where $\boldsymbol{g}_B(\boldsymbol{R}) = \hat{\boldsymbol{R}} \times \boldsymbol{g}_E(\boldsymbol{R})$ in the far field. The $E_{\rm cl}(\boldsymbol{R})$ and $B_{cl}(\boldsymbol{R})$ are proportional to the classical electric and magnetic fields from the laser. The flux in the direction $\boldsymbol{\mu}$ then has the form

$$\mathcal{F} \propto \mu \cdot {\rm Tr}[\hat{\boldsymbol{E}}^\dagger(\boldsymbol{R}) \times \hat{\boldsymbol{B}}(\boldsymbol{R})\hat{\rho} - \hat{\boldsymbol{B}}^\dagger(\boldsymbol{R}) \times \hat{\boldsymbol{E}}(\boldsymbol{R})\hat{\rho}]. \tag{17}$$

There are simpler equations for the far field involving the sum over the dipoles with appropriate phase factors. Because there are position operators in this expression, there are density matrix terms off diagonal in vibrational quantum numbers which contribute. The transmission and reflection probabilities can be calculated from the flux.

For light in one dimension, the equations simplify so that the operator

$$\hat{\tau}(x_1, x_2, \ldots) = 1 - i\frac{\Gamma}{\Omega} \sum_j \hat{\sigma}_j^- e^{-ik_0(X_j + x_j)}, \tag{18}$$

leads to the transmission probability

$$T = {\rm Tr}[\hat{\tau}^\dagger \hat{\tau} \hat{\rho}] = {\rm Tr}[\hat{\tau} \hat{\rho} \hat{\tau}^\dagger], \tag{19}$$

and the operator

$$\hat{\theta}(x_1, x_2, \ldots) = -i\frac{\Gamma}{\Omega} \sum_j \hat{\sigma}_j^- e^{ik_0(X_j + x_j)}, \tag{20}$$

leads to the reflection probability

$$R = {\rm Tr}[\hat{\theta}^\dagger \hat{\theta} \hat{\rho}] = {\rm Tr}[\hat{\theta} \hat{\rho} \hat{\theta}^\dagger]. \tag{21}$$

Note that there are the position operators x_j in both the transmission and reflection probability which can lead to connections with off-diagonal vibrational states in the density matrix.

III. SUDDEN APPROXIMATION

The sudden approximation can be quite accurate when the electronic states evolve on timescales much faster than the oscillation period of the atoms. Also, the atoms need to scatter or reflect few enough photons that they are not appreciably accelerated from the recoil. The sudden approximation was used in Refs. [71,72] and verified in Ref. [70] for photons interacting collectively with many atoms.

To explore the sudden approximation, we first transform the density matrix from the vibrational basis into the position basis using the vibrational wave functions

$$\begin{aligned}\langle \boldsymbol{r}_1, \boldsymbol{r}_2, \ldots, |\hat{\rho}|\boldsymbol{r}'_1, \boldsymbol{r}'_2, \ldots, \rangle \\ = \sum_{n_1, n_2 \ldots} \sum_{n'_1, n'_2 \ldots} \psi_{n_1}(\boldsymbol{r}_1)\psi_{n_2}(\boldsymbol{r}_2) \ldots \langle n_1| \langle n_2| \ldots \langle n_N|\hat{\rho}|n'_1\rangle|n'_2\rangle \\ \ldots |n'_N\rangle \psi_{n'_1}(\boldsymbol{r}'_1)\psi_{n'_2}(\boldsymbol{r}'_2) \ldots,\end{aligned} \tag{22}$$

with $\psi_{n_j}(\boldsymbol{r}_j)$ the vibrational wave function for atom j. At this point, there are no approximations. This form is much more difficult to use in a fully numerical treatment because many more points in real space, $\boldsymbol{r}_1, \boldsymbol{r}_2, \ldots$, are required for converged calculations compared to the vibrational states of Eq. (13). The trapping Hamiltonian in Eq. (4) leads to coherences between $\boldsymbol{r}_j$ and $\boldsymbol{r}'_j$ and the transfer of amplitude between different points in the $3N$ space. To be clear, from completeness arguments, this formulation must give the same result when converged as using the vibrational basis functions, Eq. (13).

The basic idea for the sudden *approximation* is to disregard the trapping potential and atom kinetic energy in the Hamiltonian. This still leads to a density matrix with off diagonal coherence for the positions $\mathbf{r}_j$ and $\mathbf{r}'_j$ in the left and right

sides. Also, the amplitudes at different positions evolve differently due to the position dependence of the photon-atom and dipole-dipole interactions. However, it does not involve amplitudes moving to different positions, and thus, calculations for separate values of $\boldsymbol{r}_1, \boldsymbol{r}_2, \ldots, \boldsymbol{r}'_1, \boldsymbol{r}'_2 \ldots$ can be performed independently. This method can be used to approximately calculate the recoil delivered to the atoms, giving accurate values when $\omega_t \ll \Gamma$. In fact, it is precisely these types of terms investigated in Refs. [71,72] that lead to changes in the average kinetic energy of the atoms which was verified in Ref. [70].

The position representation of the density matrix leads to simple forms of the flux, transmission probability, and reflection probability. To see this, examine the expression for the transmission probability, Eq. (19), in the position representation

$$T = \int dx_1 dx_2 \ldots \mathrm{Tr}[\hat{\tau}^\dagger(x_1, x_2, \ldots,)\hat{\tau}(x_1, x_2, \ldots,) \times \langle x_1, x_2, \ldots, |\hat{\rho}|x_1, x_2, \ldots, \rangle]. \tag{23}$$

There are no approximations in this expression.

Suppose the system starts in the ground electronic state with any type of positions coherence in the density matrix

$$\langle x_1, x_2 \ldots |\hat{\rho}|x'_1, x'_2, \ldots\rangle = \rho_0(x_1, x_2, \ldots, x'_1, x'_2 \ldots)|\mathcal{G}\rangle\langle\mathcal{G}|, \tag{24}$$

with $|\mathcal{G}\rangle$ is all electronic states in the ground state and the ρ_0 function encapsulating any positional coherences. Within the sudden approximation, the ρ_0 does not change and the electronic part of the density matrix evolves depending on the positions. Once the system reaches steady state, the electronic part goes to

$$|\mathcal{G}\rangle\langle\mathcal{G}| \to \hat{\rho}_{SA}(x_1, x_2, \ldots, x'_1, x'_2, \ldots), \tag{25}$$

with the sudden approximation density matrix the same as that calculated in Refs. [71,72]. Using this in the expressions for the flux, transmission probability, or reflection probability leads to a conceptually simple reduction. For example, the transmission probability can be written as

$$\begin{aligned} T &= \int dx_1 dx_2 \ldots \mathrm{Tr}[\hat{\tau}^\dagger(x_1, x_2, \ldots)\hat{\tau}(x_1, x_2, \ldots) \\ &\quad \times \rho_0(x_1, x_2, \ldots, x_1, x_2, \ldots)\hat{\rho}_{SA}(x_1, x_2, \ldots, x_1, x_2, \ldots)] \\ &= \int dx_1 dx_2 \ldots P(x_1, x_2, \ldots) T_{SA}(x_1, x_2 \ldots), \end{aligned} \tag{26}$$

where $P(x_1, x_2, \ldots) = \rho_0(x_1, x_2, \ldots, x_1, x_2, \ldots)$ is the initial probability density for finding atom 1 at position x_1 and atom 2 atom position $x_2 \ldots$ and the sudden approximation transmission probability

$$T_{SA}(x_1, x_2 \ldots) = \mathrm{Tr}[\hat{\tau}^\dagger(x_1, x_2, \ldots)\hat{\tau}(x_1, x_2, \ldots) \times \hat{\rho}_{SA}(x_1, x_2, \ldots, x_1, x_2, \ldots)] \tag{27}$$

is the probability for photon transmission if atom 1 is at position x_1 and atom 2 is at position x_2 and so on. A similar treatment of the flux and reflection probability leads to the same form: compute the relevant quantity (flux, transmission probability, reflection probability, etc.) for atoms fixed in space and average over their possible positions from $P(x_1, x_2, \ldots)$.

Although this result is simple, it does lead to somewhat surprising conclusions. For example, suppose all atoms start in the vibrational ground state and the parameter $\eta = k_0\sqrt{\hbar/(2M\omega_t)}$ is tiny. Since the recoil energy over the vibrational spacing is η^2, one might expect that one could use the approximation that the atoms are in the ground state throughout the evolution. As will be seen in the Sec. IV, this can qualitatively miss the changes due to the spread in positions.

Evolution timescale

The discussion of the sudden approximation depends on the duration of the light-atom interaction. Sometimes the situation involves the properties of the light once the atoms reach steady state in which case the duration is until the electronic states stop evolving. Sometimes the properties are required before the steady state is reached, which would shorten the duration. The accuracy of the sudden approximation requires the atoms to be fixed in space for this duration. By this we mean, the atom positions would not be expected to change in an important way on the timescale of the measurement of the light properties.

Weak light, $\Omega \ll \Gamma$, leads to the simplest case. For steady-state properties, the electronic states will require several lifetimes. The relevant lifetime for light coupling to superradiant states is less than $1/\Gamma$ while light coupling to subradiant states leads to relevant lifetimes larger than $1/\Gamma$. For this case, the condition will often be $(10\text{–}100)/\Gamma \ll 1/\omega_t$ depending on the extent of subradiance.

If the light is intense and/or the η becomes large, the recoil of the atoms or dipole-dipole forces can also become important. The recoil or the dipole-dipole interactions could cause the atoms to accelerate so that the atom velocity increases substantially. The atom separation divided by the increased speed then becomes the comparison timescale, not $1/\omega_t$.

Lastly, we restrict the atoms to be cold. If the atoms could be initially moving quickly, i.e., higher temperature, then the electronic states need to evolve on timescales fast compared the atom separation divided by the speed of the atoms. For this case, Doppler effects could lead to the collective light-atom interaction being relatively uninteresting.

IV. RESULTS

While the derivation of the previous section clearly shows that for the sudden approximation case, the proper procedure is to compute the flux, reflection probability, or transmission probability by fixing the atoms in space and then averaging over their positions, it is interesting to numerically examine a case that can show this result. In particular, we want to show that using the approximation that all atoms are in the ground vibrational state throughout the calculation is a qualitatively different, and sometimes inaccurate, approximation.

For atoms in free space, $N \gg 1$ to clearly distinguish between large-scale transmission and reflection. This leads to very large calculations because there will need to be at least a few vibrations for every atom. For N atoms with two internal states and $n_{\max} = N_{\mathrm{vib}} - 1$ the maximum vibrational quantum,

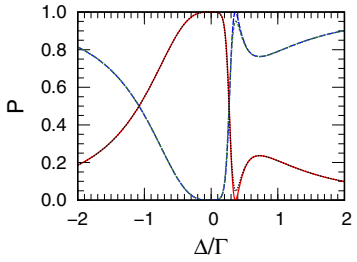

FIG. 1. The transmission T and reflection R probabilities for the one-dimensional case discussed in the text. For the case where the separation d of the atoms is exactly 0.9λ, the red solid (blue long dash) line is the R (T) probability. When the average separation $\langle d\rangle$ is 0.9λ, but the positions are averaged over the vibrational ground state, the black dotted (green dash) is the R (T) probability.

there are $[2N_{\rm vib}]^{2N}$ terms in the density matrix. Fortunately, the one-dimensional example can have transmission and reflection probabilities that strongly depend on the atom separations for two atoms when the average separation is near an integer number of wavelengths. This allows a fully numerical simulation with modest computational resources.

The one-dimensional case with two atoms near an integer wavelength separation has a subradiant interference feature leading to a relatively sharp transmission peak. The position and width of the transmission peak depend strongly on the actual separation so a spread in atom positions can lead to a clear change.

The results in Figs. 1 and 2 are for two atoms interacting through a one-dimensional wave guide, Eqs. (10) and (11). To ensure that we satisfied the conditions for the sudden approximation, we chose somewhat extreme parameters: $\Gamma = 2\pi\,10\,\text{MHz}$, $\Omega = 10^{-4}\Gamma$, $\lambda = 3.1\,\text{mm}$, $d = 0.9\lambda$, $M = 1.6605\times10^{-28}\,\text{kg}$, $\omega_t = 10^3\ \text{s}^{-1}$. This leads to $\eta \simeq 0.036$ and a recoil energy over vibrational spacing of $\eta^2 \simeq 0.0013$. Because there are two atoms in their ground vibrational state, the standard deviation of the separation is $\sigma = \sqrt{\hbar/(M\omega_t)}$ leading to $\sigma/\lambda = \eta/(\pi\sqrt{2}) \simeq 0.0081$. Figure 1 compares the transmission T and reflection R probabilities versus detuning for the perfect separation and from averaging over the positions of the atoms in their vibrational ground state. For most of the range of detuning Δ averaging over the atoms' positions has little effect. The largest effect from averaging is near $\Delta = 0.36\Gamma$ where the interference leads to a sharp peak in the transmission probability. The effect is large for that detuning because the position and width of the transmission peak strongly depends on the value of the separation when the separation $d \sim \lambda$.

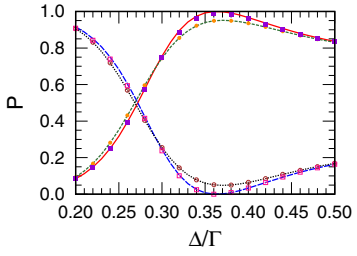

FIG. 2. Same as Fig. 1 but also showing the results of the restricted quantum calculation with $n_{\rm max} = 0$ (purple solid square for T, empty pink square for R) and the converged quantum calculation restricted with $n_{\rm max} = 4$ for both atoms (orange solid circle for T, maroon empty circle for R).

Figure 2 is the same plot over a smaller range of detuning with the results from two full quantum calculations, Eqs. (19) and (21), with a different number of vibrational states. The quantum calculation that restricted all vibrations to be in the ground state, $n_{\rm max} = 0$, has the purple solid square for T and the empty pink square for R. These values are in decent agreement with the calculation that *does not average* over the atoms' positions. However, the transmission plus reflection probabilities for this approximation only adds up to 0.990 at $\Delta = 0.36\Gamma$ indicating there is a lack of convergence. By increasing $n_{\rm max}$, we can demonstrate convergence of the quantum calculation. In Fig. 2, the $n_{\rm max} = 4$ results are orange solid circle for T and maroon empty circle for R which are in excellent agreement with the simple spatial averaging. The largest difference is near $\Delta = 0.36\Gamma$. At this value of detuning, the sum of reflection and transmission probabilities give $1 - R - T \simeq 4.6\times10^{-7}$, and the difference between the simple spatial averaging and the quantum calculation of the transmission probability was $\sim 3\times10^{-6}$. This demonstrates that, even though the ratio of recoil energy to vibrational energy spacing is tiny, $\eta^2 \sim 0.0013$, one cannot restrict the calculation to the vibrational ground state.

We perform calculations for $d = 0.95\lambda$ and $\omega_t = 4\times10^3\ \text{s}^{-1}$ with everything else kept the same. This decreases the change from integer lambda spacing by a factor of 2 from 0.1 to 0.05 which makes the subradiant state lifetime approximately four times longer. By increasing ω_t by a factor of 4, the η decreases by a factor of 2. This keeps the $\sigma/\Delta\lambda$ the same. We find the same trends as in Fig. 2 with the $n_{\rm max} = 0$ in good agreement with the $d = 0.95\lambda$ curve and the $n_{\rm max} = 4$ in excellent agreement with the spatially averaged results. This case has a larger change in probabilities due to averaging: the maximum for T after averaging is $\simeq 0.842$. The $n_{\rm max} = 0$ calculation has a maximum for T of 0.98. Note that decreasing η means the ratio of recoil energy to vibrational energy spacing decreased by a factor of 4 to $\eta^2 \simeq 3.3\times10^{-4}$ which might make it even more surprising that the $n_{\rm max} = 0$ calculation gets the change in probabilities so wrong.

Changing the wavelength to $\lambda = 2\,\text{mm}$, leads to $\eta \simeq 0.056$ and $\sigma/\lambda \simeq 0.0126$. This gives a spread of positions that is 1.55 times larger than the calculations in Figs. 1 and 2 which will lead to a larger effect from averaging. The results are shown in Fig. 3 where it is clear that spatial averaging has a larger effect. In the plot are shown the points for calculations with $n_{\rm max} = 0$, 1, and 2 where it is clear that most of the change occurs when going from 0 to 1. In fact, for both the $\lambda = 3.1$ and 2 mm calculations, the $n_{\rm max} = 1$ results are good enough to reach better than 1% accuracy. For the 2-mm calculation at $\Delta = 0.36\Gamma$, going from $n_{\rm max} = 0$ to 1 to 2 gives $1 - R - T$ going from 2.4×10^{-2} to 2.3×10^{-3} to 3.7×10^{-4} and an error in T going from 8.0×10^{-2} to -6.4×10^{-3} to 5.4×10^{-4}.

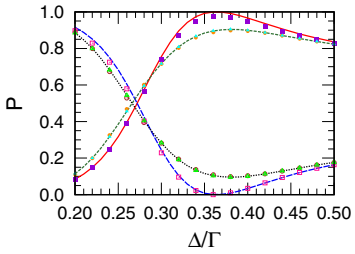

FIG. 3. Similar to Fig. 2 but for $\lambda = 2\,\text{mm}$ which increases the relative size of the averaging region. The red solid (blue long dash) line is the R (T) probability for perfect separation while the black dotted (green dash) spatially average the positions. The results of the $n_{\max} = 0$ (purple solid square for T, empty pink square for R), $n_{\max} = 1$ (orange solid circle for T, maroon empty circle for R), and $n_{\max} = 2$ (turquoise solid triangle for T, empty green triangle for R).

We repeat the calculations that use $\lambda = 2\,\text{mm}$ but with three atoms to ensure there was nothing special about the two-atom case. Because there are more atoms, the separation does not need to be as close to an integer wavelength to get sensitivity to the atom positions. In Fig. 4, we show the transmission and reflection probability versus detuning for three atoms with average separation of $d = 0.85\lambda$. The line and point types are the same as Fig. 3. As with the previous plot, these show the very strong error for the calculation with $n_{\max} = 0$ and progressive convergence toward the spatial averaging result with increasing $n_{\max}$. At $\Delta = 0.36\Gamma$, going from $n_{\max} = 0$ to 1 to 2 to 3 gives $1 - R - T$ going from 6.3×10^{-2} to 3.1×10^{-3} to 7.7×10^{-4} to 1.3×10^{-4} and an error in T going from 5.4×10^{-2} to -5.3×10^{-3} to 2.0×10^{-4} to -6.6×10^{-5}.

The sudden approximation can be made to fail by having the trap frequency ω_t increase. However, changing the trap frequency alone causes other basic parameters to change. Importantly, increasing ω_t decreases the spread of the wave function. One could keep the spread fixed by inversely changing the mass, M. For example, increasing ω_t by a factor of 10 and decreasing M by a factor of 10. Another method would be to change Γ and Ω keeping their ratio fixed. Both methods lead to the same reflection and transmission probabilities when ω_t/Γ is the same in each method. Figure 5 shows the result for $\lambda = 2\,\text{mm}$ and $\eta \simeq 0.056$. The $\omega_t = 10^5$ and $10^6\ \text{s}^{-1}$ give nearly the same result as the previous case where $\omega_t = 10^3\ \text{s}^{-1}$ which closely matches the spatial average. However,

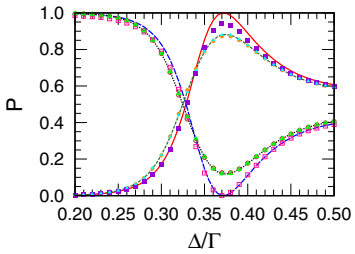

FIG. 4. Same as Fig. 3 but for three atoms with a separation of $d = 0.85\lambda$.

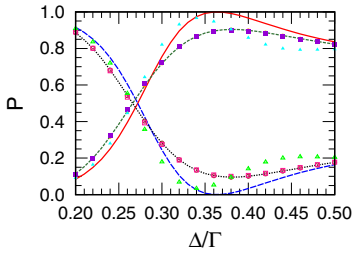

FIG. 5. Similar to Fig. 3 but for different ω_t with the M inversely changed to keep $\sigma = \sqrt{\hbar/(M\omega_t)}$ unchanged. The results of the $n_{\max} = 4$ for $\omega_t = 10^5\ \text{s}^{-1}$ (orange solid circle for T, maroon empty circle for R), $10^6\ \text{s}^{-1}$ (purple solid square for T, empty pink square for R), and $10^7\ \text{s}^{-1}$ (turquoise solid triangle for T, empty green triangle for R).

the $\omega_t = 10^7\ \text{s}^{-1}$ result is substantially different. For this trap frequency, the decay time, $1/\Gamma$ is still a small fraction of the trap period $2\pi/\omega_t$. However, the proper comparison is between the trap period and the lifetime of the subradiant excitation which are comparable.

The sudden approximation also can be made to fail for larger values of the Rabi frequency, Ω. We repeat the calculations for the parameters of Fig. 3 but with $\Omega = 10^{-3}$, 0.01, and 0.1Γ. All of these cases have $\Omega \gg \omega_t$, and, for the fixed atom calculations, lead to steady-state results for times much less than $1/\omega_t$. Except for the $\Omega = \Gamma/10$ case, the simple spatial averaging gives an excellent approximation to the converged vibrational calculation. However, the $\Omega = \Gamma/10$ case gives qualitatively different results between the simple spatial averaging and the converged vibrational calculation because the atoms substantially shift positions under the radiation pressure from the reflected and scattered photons.

V. SUMMARY

We explore the role that spatial averaging plays in the reflection or transmission of photons through atom arrays. In experiments, the atoms will be held in space using trapping lasers leading to a spread in atom positions which affects the transmission and reflection properties. We envision situations where the light intensity is low enough that the trap energy of the atoms hardly changes.

Using the sudden approximation and fully numerical calculations, we show that simply averaging the reflection and transmission over the atom positions is accurate when the trap period is much larger than the evolution timescale of the electronic states. This approximation breaks down when the trap period is comparable to or shorter than the electronic state evolution timescale or for high intensity where the atom velocity and position change due to radiation pressure or dipole-dipole forces.

ACKNOWLEDGMENTS

I am grateful to Chen-Lung Hung for suggesting this question and discussions with Deepak Suresh. This work was supported by the U.S. National Science Foundation under

Grant No. 2410890-PHY and through a grant for ITAMP at Harvard University.

DATA AVAILABILITY

The data plotted in the figures are available in Ref. [73].

APPENDIX: EVALUATION OF VIBRATIONAL MATRIX ELEMENTS

The differential equations for the density matrix requires the evaluation of matrix elements of complicated functions involving different vibrational levels. In the limit that η is small, these matrix elements are often evaluated using a power series technique. For example, evaluating a matrix element of a function of the operator $\hat{x}$ could use an approximation like

$$\langle n|F(X+\hat{x})|n'\rangle = F(X)\langle n|n'\rangle + F'(X)\langle n|\hat{x}|n'\rangle, \tag{A1}$$

which stops at first order in the expansion. A better approximation would continue to second (or higher) order in $\hat{x}$. However, when F is a complicated function, the evaluation of higher derivatives can be complicated and are often discarded for third and higher order.

We use a discrete variable method for evaluation of matrix elements of complicated functions [74]. The idea is to find the eigenvalues and eigenvectors of the matrix of the $\hat{x}$ operator and use those to evaluate the matrix elements. For a finite basis set from 0 to $n_{\rm fin}$, find

$$\sum_{n'=0}^{n_{\rm fin}} \langle n|\hat{x}|n'\rangle U_{n'\beta} = U_{n\beta} x_\beta, \tag{A2}$$

where U is the unitary matrix of eigenvectors and x_β are the eigenvalues. The matrix elements are approximately given by

$$\langle n|F(X+\hat{x})|n'\rangle \simeq \sum_\beta U_{n\beta} F(X+x_\beta) U^\dagger_{\beta n'}, \tag{A3}$$

where the accuracy increases for larger $n_{\rm fin}$.

There are many advantages of this method of which we will give three: (1) the computation of the derivatives of F is unnecessary; (2) if F is a unitary operator, the resulting matrix will be exactly unitary if $n_{\rm fin}$ matches the $n_{\rm max}$ in the calculation; and (3) for harmonic oscillator basis functions and the $\hat{x}$ operator, the $\langle n|\hat{x}|n'\rangle$ is tridiagonal leading to the equivalent of high-order Taylor series expansion of F for the small n, n' matrix elements.

[1] D. E. Chang, J. Ye, and M. D. Lukin, Controlling dipole-dipole frequency shifts in a lattice-based optical atomic clock, Phys. Rev. A **69**, 023810 (2004).

[2] L. Henriet, J. S. Douglas, D. E. Chang, and A. Albrecht, Critical open-system dynamics in a one-dimensional optical-lattice clock, Phys. Rev. A **99**, 023802 (2019).

[3] C. Qu and A. M. Rey, Spin squeezing and many-body dipolar dynamics in optical lattice clocks, Phys. Rev. A **100**, 041602 (2019).

[4] D. E. Chang, L. Jiang, A. V. Gorshkov, and H. J. Kimble, Cavity QED with atomic mirrors, New J. Phys. **14**, 063003 (2012).

[5] S. D. Jenkins and J. Ruostekoski, Controlled manipulation of light by cooperative response of atoms in an optical lattice, Phys. Rev. A **86**, 031602(R) (2012).

[6] R. T. Sutherland and F. Robicheaux, Collective dipole-dipole interactions in an atomic array, Phys. Rev. A **94**, 013847 (2016).

[7] G. Facchinetti, S. D. Jenkins, and J. Ruostekoski, Storing light with subradiant correlations in arrays of atoms, Phys. Rev. Lett. **117**, 243601 (2016).

[8] E. Shahmoon, D. S. Wild, M. D. Lukin, and S. F. Yelin, Cooperative resonances in light scattering from two-dimensional atomic arrays, Phys. Rev. Lett. **118**, 113601 (2017).

[9] J. Perczel, J. Borregaard, D. E. Chang, H. Pichler, S. F. Yelin, P. Zoller, and M. D. Lukin, Photonic band structure of two-dimensional atomic lattices, Phys. Rev. A **96**, 063801 (2017).

[10] J. Perczel, J. Borregaard, D. E. Chang, H. Pichler, S. F. Yelin, P. Zoller, and M. D. Lukin, Topological quantum optics in two-dimensional atomic arrays, Phys. Rev. Lett. **119**, 023603 (2017).

[11] R. J. Bettles, J. Minář, C. S. Adams, I. Lesanovsky, and B. Olmos, Topological properties of a dense atomic lattice gas, Phys. Rev. A **96**, 041603(R) (2017).

[12] A. Asenjo-Garcia, H. J. Kimble, and D. E. Chang, Optical waveguiding by atomic entanglement in multilevel atom arrays, Proc. Natl. Acad. Sci. USA **116**, 25503 (2019).

[13] J. A. Needham, I. Lesanovsky, and B. Olmos, Subradiance-protected excitation transport, New J. Phys. **21**, 073061 (2019).

[14] Y.-X. Zhang and K. Mølmer, Theory of subradiant states of a one-dimensional two-level atom chain, Phys. Rev. Lett. **122**, 203605 (2019).

[15] S. J. Masson, I. Ferrier-Barbut, L. A. Orozco, A. Browaeys, and A. Asenjo-Garcia, Many-body signatures of collective decay in atomic chains, Phys. Rev. Lett. **125**, 263601 (2020).

[16] J. Javanainen and R. Rajapakse, Light propagation in systems involving two-dimensional atomic lattices, Phys. Rev. A **100**, 013616 (2019).

[17] M. Moreno-Cardoner, D. Plankensteiner, L. Ostermann, D. E. Chang, and H. Ritsch, Subradiance-enhanced excitation transfer between dipole-coupled nanorings of quantum emitters, Phys. Rev. A **100**, 023806 (2019).

[18] L. A. Williamson and J. Ruostekoski, Optical response of atom chains beyond the limit of low light intensity: The validity of the linear classical oscillator model, Phys. Rev. Res. **2**, 023273 (2020).

[19] R. J. Bettles, M. D. Lee, S. A. Gardiner, and J. Ruostekoski, Quantum and nonlinear effects in light transmitted through planar atomic arrays, Commun. Phys. **3**, 141 (2020).

[20] K. E. Ballantine and J. Ruostekoski, Optical magnetism and Huygens' surfaces in arrays of atoms induced by cooperative responses, Phys. Rev. Lett. **125**, 143604 (2020).

[21] S. J. Masson and A. Asenjo-Garcia, Atomic-waveguide quantum electrodynamics, Phys. Rev. Res. **2**, 043213 (2020).

[22] K. E. Ballantine and J. Ruostekoski, Cooperative optical wavefront engineering with atomic arrays, Nanophotonics **10**, 1901 (2021).

[23] D. Cano, Photon statistics of the light transmitted and reflected by a two-dimensional atomic array, Phys. Rev. A **104**, 053709 (2021).

[24] F. Robicheaux, Theoretical study of early-time superradiance for atom clouds and arrays, Phys. Rev. A **104**, 063706 (2021).

[25] K. E. Ballantine and J. Ruostekoski, Quantum single-photon control, storage, and entanglement generation with planar atomic arrays, PRX Quantum **2**, 040362 (2021).
[26] O. Rubies-Bigorda and S. F. Yelin, Superradiance and subradiance in inverted atomic arrays, Phys. Rev. A **106**, 053717 (2022).
[27] S. J. Masson and A. Asenjo-Garcia, Universality of Dicke superradiance in arrays of quantum emitters, Nat. Commun. **13**, 2285 (2022).
[28] E. Sierra, S. J. Masson, and A. Asenjo-Garcia, Dicke superradiance in ordered lattices: Dimensionality matters, Phys. Rev. Res. **4**, 023207 (2022).
[29] M. Moreno-Cardoner, R. Holzinger, and H. Ritsch, Efficient nano-photonic antennas based on dark states in quantum emitter rings, Opt. Express **30**, 10779 (2022).
[30] C.-R. Mann and E. Mariani, Topological transitions in arrays of dipoles coupled to a cavity waveguide, Phys. Rev. Res. **4**, 013078 (2022).
[31] R. Gutiérrez-Jáuregui and A. Asenjo-Garcia, Coherent control in atomic chains: to trap and release a traveling excitation, Phys. Rev. Res. **4**, 013080 (2022).
[32] D. Fernández-Fernández and A. González-Tudela, Tunable directional emission and collective dissipation with quantum metasurfaces, Phys. Rev. Lett. **128**, 113601 (2022).
[33] V. Walther, L. Zhang, S. F. Yelin, and T. Pohl, Nonclassical light from finite-range interactions in a two-dimensional quantum mirror, Phys. Rev. B **105**, 075307 (2022).
[34] M. B. de Paz, A. González-Tudela, and P. A. Huidobro, Manipulating generalized Dirac cones in subwavelength dipolar arrays, Phys. Rev. A **106**, 033505 (2022).
[35] Y.-C. Wang, J.-S. You, and H.-H. Jen, A non-hermitian optical atomic mirror, Nat. Commun. **13**, 4598 (2022).
[36] S. P. Pedersen, L. Zhang, and T. Pohl, Quantum nonlinear metasurfaces from dual arrays of ultracold atoms, Phys. Rev. Res. **5**, L012047 (2023).
[37] M. B. de Paz and P. A. Huidobro, Bound states in the continuum in subwavelength emitter arrays, Phys. Rev. Res. **5**, 033108 (2023).
[38] N. Fayard, I. Ferrier-Barbut, A. Browaeys, and J.-J. Greffet, Optical control of collective states in one-dimensional ordered atomic chains beyond the linear regime, Phys. Rev. A **108**, 023116 (2023).
[39] Y. Solomons and E. Shahmoon, Multichannel waveguide QED with atomic arrays in free space, Phys. Rev. A **107**, 033709 (2023).
[40] V. Scheil, R. Holzinger, M. Moreno-Cardoner, and H. Ritsch, Optical properties of concentric nanorings of quantum emitters, Nanomaterials **13**, 851 (2023).
[41] S. Ostermann, O. Rubies-Bigorda, V. Zhang, and S. F. Yelin, Breakdown of steady-state superradiance in extended driven atomic arrays, Phys. Rev. Res. **6**, 023206 (2024).
[42] C.-H. Wang, N.-Y. Tsai, Y.-C. Wang, and H. H. Jen, Light-scattering properties beyond weak-field excitation in atomic ensembles, Phys. Rev. A **110**, 013708 (2024).
[43] R. Ben-Maimon, Y. Solomons, and E. Shahmoon, Dissipative transfer of quantum correlations from light to atomic arrays, Phys. Rev. A **110**, 033719 (2024).
[44] M. Cech, I. Lesanovsky, and B. Olmos, Dispersionless subradiant photon storage in one-dimensional emitter chains, Phys. Rev. A **108**, L051702 (2023).
[45] T. L. Patti, D. S. Wild, E. Shahmoon, M. D. Lukin, and S. F. Yelin, Controlling interactions between quantum emitters using atom arrays, Phys. Rev. Lett. **126**, 223602 (2021).
[46] A. Asenjo-Garcia, M. Moreno-Cardoner, A. Albrecht, H. J. Kimble, and D. E. Chang, Exponential improvement in photon storage fidelities using subradiance and "selective radiance" in atomic arrays, Phys. Rev. X **7**, 031024 (2017).
[47] M.T. Manzoni, M. Moreno-Cardoner, A. Asenjo-Garcia, J. V. Porto, A. V. Gorshkov, and D. E. Chang, Optimization of photon storage fidelity in ordered atomic arrays, New J. Phys. **20**, 083048 (2018).
[48] P.-O. Guimond, A. Grankin, D. V. Vasilyev, B. Vermersch, and P. Zoller, Subradiant Bell states in distant atomic arrays, Phys. Rev. Lett. **122**, 093601 (2019).
[49] R. Bekenstein, I. Pikovski, H. Pichler, E. Shahmoon, S. F. Yelin, and M. D. Lukin, Quantum metasurfaces with atom arrays, Nat. Phys. **16**, 676 (2020).
[50] A. Cidrim, T. S. do Espirito Santo, J. Schachenmayer, R. Kaiser, and R. Bachelard, Photon blockade with ground-state neutral atoms, Phys. Rev. Lett. **125**, 073601 (2020).
[51] S. Buckley-Bonanno, S. Ostermann, O. Rubies-Bigorda, T. L. Patti, and S. F. Yelin, Optimized geometries for cooperative photon storage in an impurity coupled to a two-dimensional atomic array, Phys. Rev. A **106**, 053706 (2022).
[52] K. E. Ballantine and J. Ruostekoski, Unidirectional absorption, storage, and emission of single photons in a collectively responding bilayer atomic array, Phys. Rev. Res. **4**, 033200 (2022).
[53] O. Rubies-Bigorda, V. Walther, T. L. Patti, and S. F. Yelin, Photon control and coherent interactions via lattice dark states in atomic arrays, Phys. Rev. Res. **4**, 013110 (2022).
[54] Y.-X. Han, H. Chen, W. Liu, J.-J. Xue, and H.-R. Li, Optimal subradiant spin wave exchange in dipole-coupled atomic ring arrays, New J. Phys. **25**, 103008 (2023).
[55] F. Shah, T. L. Patti, O. Rubies-Bigorda, and S. F. Yelin, Quantum computing with subwavelength atomic arrays, Phys. Rev. A **109**, 012613 (2024).
[56] Z. Meir, O. Schwartz, E. Shahmoon, D. Oron, and R. Ozeri, Cooperative Lamb shift in a mesoscopic atomic array, Phys. Rev. Lett. **113**, 193002 (2014).
[57] A. Grankin, P.-O. Guimond, D. V. Vasilyev, B. Vermersch, and P. Zoller, Free-space photonic quantum link and chiral quantum optics, Phys. Rev. A **98**, 043825 (2018).
[58] R. J. Bettles, S. A. Gardiner, and C. S. Adams, Enhanced optical cross section via collective coupling of atomic dipoles in a 2D array, Phys. Rev. Lett. **116**, 103602 (2016).
[59] D. E. Chang, J. S. Douglas, A. González-Tudela, C.-L. Hung, and H. J. Kimble, Colloquium: Quantum matter built from nanoscopic lattices of atoms and photons, Rev. Mod. Phys. **90**, 031002 (2018).
[60] L. A. Williamson, M. O. Borgh, and J. Ruostekoski, Superatom picture of collective nonclassical light emission and dipole blockade in atom arrays, Phys. Rev. Lett. **125**, 073602 (2020).
[61] J. Rui, D. Wei, A. Rubio-Abadal, S. Hollerith, J. Zeiher, D. M. Stamper-Kurn, C. Gross, and I. Bloch, A subradiant optical mirror formed by a single structured atomic layer, Nature (London) **583**, 369 (2020).
[62] R. Gutiérrez-Jáuregui and A. Asenjo-Garcia, Directional transport along an atomic chain, Phys. Rev. A **105**, 043703 (2022).

[63] S. Ribeiro and S. A. Gardiner, Quantum emission of light with densely packed driven dipoles, Phys. Rev. A **105**, L021701 (2022).

[64] O. Rubies-Bigorda, S. Ostermann, and S. F. Yelin, Characterizing superradiant dynamics in atomic arrays via a cumulant expansion approach, Phys. Rev. Res. **5**, 013091 (2023).

[65] N. S. Baßler, M. Reitz, K. P. Schmidt, and C. Genes, Linear optical elements based on cooperative subwavelength emitter arrays, Opt. Express **31**, 6003 (2023).

[66] K. Srakaew, P. Weckesser, S. Hollerith, D. Wei, D. Adler, I. Bloch, and J. Zeiher, A subwavelength atomic array switched by a single Rydberg atom, Nat. Phys. **19**, 714 (2023).

[67] Y. Solomons, R. Ben-Maimon, and E. Shahmoon, Universal approach for quantum interfaces with atomic arrays, PRX Quantum **5**, 020329 (2024).

[68] J. Ruostekoski, Cooperative quantum-optical planar arrays of atoms, Phys. Rev. A **108**, 030101 (2023).

[69] A. S. Sheremet, M. I. Petrov, I. V. Iorsh, A. V. Poshakinskiy, and A. N. Poddubny, Waveguide quantum electrodynamics: Collective radiance and photon-photon correlations, Rev. Mod. Phys. **95**, 015002 (2023).

[70] D. A. Suresh and F. Robicheaux, Atom recoil in collectively interacting dipoles using quantized vibrational states, Phys. Rev. A **105**, 033706 (2022).

[71] F. Robicheaux and S. Huang, Atom recoil during coherent light scattering from many atoms, Phys. Rev. A **99**, 013410 (2019).

[72] D. A Suresh and F. Robicheaux, Photon-induced atom recoil in collectively interacting planar arrays, Phys. Rev. A **103**, 043722 (2021).

[73] Data for: Spatial averaging for light reflection and transmission through cold-atom arrays, https://doi.org/10.4231/5WVE-2D38.

[74] J. V. Lill, G. A. Parker, and J. C. Light, Discrete variable representations and sudden models in quantum scattering theory, Chem. Phys. Lett. **89**, 483 (1982).